Acta Crystallographica Section F
Structural Biology and Crystallization Communications
ISSN 1744-3091

Bin Liu, V. Mitch Luna, Ying Chen, C. David Stout* and James A. Fee*

The Scripps Research Institute, Department of Molecular Biology, MB-8, 10550 North Torrey Pines Road, La Jolla CA 92037, USA

Correspondence e-mail: dave@scripps.edu, jafee@scripps.edu

Received 17 August 2007
Accepted 29 October 2007

An unexpected outcome of surface engineering an integral membrane protein: improved crystallization of cytochrome ba_3 from *Thermus thermophilus*

Past work has shown that it is feasible to mutate surface residues of soluble proteins and to a lesser extent membrane proteins in order to improve their crystallization behavior. Described here is a successful application of this approach to the integral membrane protein *Thermus thermophilus* cytochrome ba_3 oxidase. Two mutant forms of this enzyme (I-K258R and I-K258R/II-E4Q) were created in which symmetrical crystal contacts within crystals of wild-type enzyme were modified. These mutant proteins had greatly shortened crystallization times, decreasing from ~30 d for the wild type to 1–3 d for the mutants, and crystallization was highly reproducible. Native-like proteins crystallize in space group $P4_32_12$, whereas the mutant proteins crystallize in space group $P4_12_12$ with a different packing arrangement. Crystals of the $P4_32_12$ form occasionally diffracted to 2.4–2.3 Å resolution following controlled dehydration, while those of the $P4_12_12$ form routinely diffracted to between 3.0 and 2.6 Å for crystals that had been cryoprotected but not dehydrated.

1. Introduction

Cytochrome *c* oxidases are integral membrane enzymes that serve as terminal respiratory complexes (Michel *et al.*, 1998). One member of this family is the cytochrome ba_3 obtained from *Thermus thermophilus* cells grown at low $p(O_2)$. An expression system permits the preparation of mutant forms of this enzyme (Chen *et al.*, 2005). Both native (Soulimane *et al.*, 2000) and recombinant wild-type enzymes (Hunsicker-Wang *et al.*, 2005) have been crystallized in space group $P4_32_12$ and structures have been reported at 2.4–2.3 Å resolution (Soulimane *et al.*, 2000; Hunsicker-Wang *et al.*, 2005). Because of difficulties in several steps of the preparation of such crystals of cyctochrome ba_3 (Soulimane *et al.*, 2003), neither is suitable for the examination of intermediates in dioxygen reduction, which requires many high-quality reproducibly formed crystals. The problems with the $P4_32_12$ crystal form include extended growth times of ~30 d, low yield, with few droplets producing crystals, and the requirement for complicated procedures to elicit useful diffraction.

There have been numerous reports on the improved crystallization of soluble proteins by surface modification (Lawson *et al.*, 1991; Takeda *et al.*, 1995; Longenecker *et al.*, 2001; Mateja *et al.*, 2002; Czepas *et al.*, 2004; D'Arcy *et al.*, 1999; Schlatter *et al.*, 2005; Mittl *et al.*, 1994; Dasgupta *et al.*, 1997, Derewenda, 2004*a*,*b*; Derewenda & Vekilov, 2006; Cooper *et al.*, 2007), in which contacts involving arginine and glutamine are favored. Crystallization of membrane proteins depends on accommodating a protein–detergent micelle in a lattice mediated by specific contacts between residues in hydrophilic domains (Ostermeier & Michel, 1997). Examples of crystalline membrane proteins reveal that only a small fraction of the exterior surface of the protein participates in intermolecular contacts (see below). To facilitate crystallization, Michel and coworkers increased the hydrophilic surface area by cocrystallizing *Paracoccus denitrificans* cytochrome aa_3 bound to a monoclonal antibody fragment (Ostermeier *et al.*, 1995, 1997; Hunte & Michel, 2002). Yu and coworkers described crystals of mutated cytochrome bc_1 complex from *Rhodobacter sphaeroides* that had improved diffraction (Elberry *et al.*, 2006). Pauth *et al.* (1999) reported modifications to the bacterial outer membrane proteins OmpA and OmpX that promoted

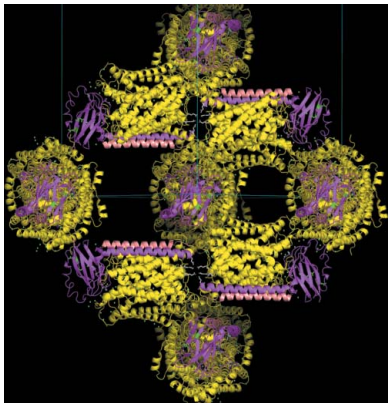

both crystallization and diffraction (see §3). In this study, we describe attempts to improve the crystallization and diffraction characteristics of *T. thermophilus* cytochrome ba_3.

2. Materials and methods

2.1. Site-directed mutagenesis

The mutations I-K258R and II-E4Q (where I and II designate subunits I and II of the enzyme) were constructed using the QuikChange site-directed mutagenesis kit from Strategene. The oligonucleotide primer pairs (Proligo) were 5′-GCAGGCCGGG-GGG**AGG**CTGGTCTCCGAC-3′ and 5′-GTCGGAGACCAG**CCT**-CCCCCCGGCCTGC-3′ for the mutation I-K258R (...QAGG**K**L-VSD...) found on the *Ppmu*I/*Bsu*36I fragment and 5′-GTAGG-TATGGTGGAC**CAG**CACAAGGCCCAC-3′ and 5′-GTGGGCCT-TGTG**CTG**GTCCACCATACCTAC-3′ for the mutation II-E4Q (MVD**E**HKAH...) found on the *Kpn*I/*Sfi*I fragment (see Fig. 5 of Chen *et al.*, 2005). All sequences were confirmed at the DNA level (TSRI Center for Nucleic Acids Research).

2.2. Protein techniques

The two mutant *T. thermophilus* cytochrome ba_3 molecules were expressed, purified and assayed as described previously (Chen *et al.*, 2005). Protein concentrations were determined using $\Delta\varepsilon_{560-590}$ = 26 000 M^{-1} cm^{-1}.

Detergent exchange was conducted on DEAE resin (GE Science) in a 1.5 × ∼5 cm column equilibrated with five column volumes of buffer *A* (10 m*M* bis-tris pH 7.0, 13 m*M* *n*-nonyl β-D-glucopyranoside from Anatrace). The enzyme was applied onto the column in bis-Tris pH 7.0, 0.05%(*w*/*v*) *n*-dodecyl β-D-glucopyranoside (Anatrace) and washed with five column volumes of buffer *A*. The protein was eluted with 10 m*M* bis-Tris pH 7.0, 0.1 *M* KCl and 13 m*M* *n*-nonyl β-D-glucopyranoside (2× CMC). The mutant proteins crystallized under the same conditions as the wild-type enzyme (Hunsicker-Wang *et al.*, 2005). Typically, the protein was concentrated to ∼20 mg ml^{-1} in 10 m*M* bis-Tris pH 7.0, 100 m*M* KCl, 13 m*M* *n*-nonyl β-D-glucopyranoside. The well solution consisted of 30 m*M* bis-Tris pH 7.0, 13–15% PEG 2K. Each droplet was formed from 2 µl protein solution plus 2 µl well solution, yielding the following condition: 6.5–7.5% PEG 2K, 50 m*M* KCl, 20 m*M* bis-Tris pH 7.0, 6.5 m*M* *n*-nonyl β-D-glucopyranoside. For the mutant crystals, the cryoprotectant was 50% 2-methyl-2,4-pentanediol, 14%(*w*/*v*) PEG 2K, 0.1 *M* KCl, 13 m*M* *n*-nonyl β-D-glucopyranoside and 0.5 *M* sodium ascorbate (Sigma–Aldrich) in 0.1 *M* bis-Tris pH 7.0.

Table 1
Data-collection and refinement statistics.

Values in parentheses are for the last shell.

	I-K258R	I-K258R/II-E4Q
Resolution (Å)	3.25 (3.43–3.25)	3.00 (3.16–3.00)
Space group	$P4_12_12$	$P4_12_12$
Unit-cell parameters (Å)	$a = b = 115.19$, $c = 149.14$	$a = b = 114.64$, $c = 148.57$
Total no. of observations	44490	77667
Unique reflection set	13540	19803
Redundancy	3.3 (3.8)	3.9 (4.2)
Completeness (%)	82.8 (82.8)	97.0 (97.0)
$I/\sigma(I)$	18.1 (1.2)	13.1 (1.1)
R_{merge}† (%)	3.2 (61.8)	5.2 (72.4)
R.m.s. deviations		
Bond lengths (Å)	0.023	0.020
Bond angles (°)	2.62	2.31
R_{work}/R_{free}‡ (%)	21.5/30.7	23.4/30.2

† $R_{merge} = \sum_{hkl}\sum_i |I_i(hkl) - \overline{I(hkl)}|/\sum_{hkl}\sum_i I_i(hkl)$, where $I_i(hkl)$ is the intensity of the ith measurement of reflection hkl and $I(hkl)$ is the mean value of $I_i(hkl)$ for all i measurements. ‡ R_{free} is the conventional crystallographic R factor, R_{work}, but calculated using 5% of the data that were excluded from the refinement.

2.3. X-ray data collection and structure determination

Data were collected at 100 K on beamline 9-1 at the Stanford Synchrotron Radiation Laboratory (SSRL) with 0.979 Å X-radiation and an ADSC Q315 CCD detector. Data were processed with *MOSFLM* (Leslie, 1999) and *SCALA* (Collaborative Computational Project, Number 4, 1994). The wild-type recombinant structure (PDB code 1xme) was used for molecular-replacement calculations with *Phaser* (Read, 2001) and refinement was performed using *REFMAC*5 (Murshudov *et al.*, 1997). Data-collection and refinement statistics are shown in Table 1. Figures were created using *PyMOL* (DeLano, 2002).

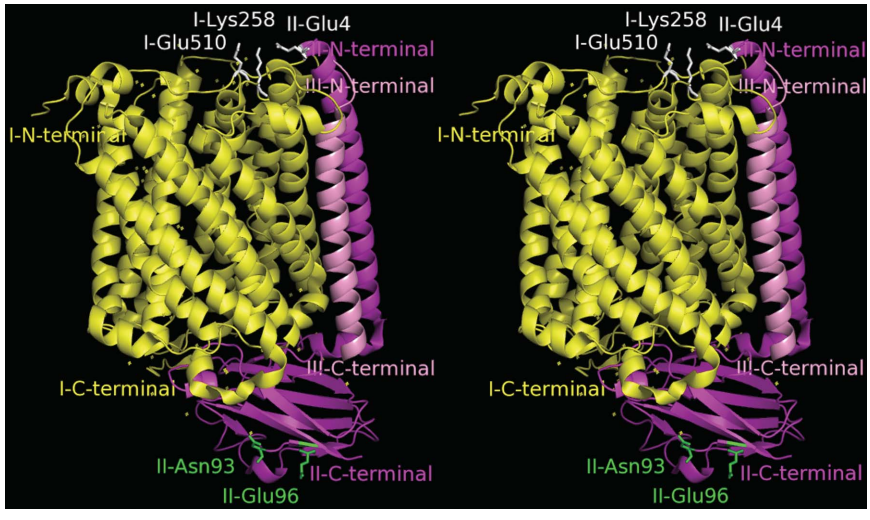

Figure 1
Stereoview (cross-eyed) of the wild-type recombinant cytochrome ba_3 from *T. thermophilus*: yellow, subunit I; magenta, subunit II; pink, subunit IIa. N- and C-termini are labeled. I-Lys258, I-Glu510 and II-Glu4 are shown as white sticks and II-Glu96 and II-Asn93 are shown as green sticks and can also be observed in Fig. 3.

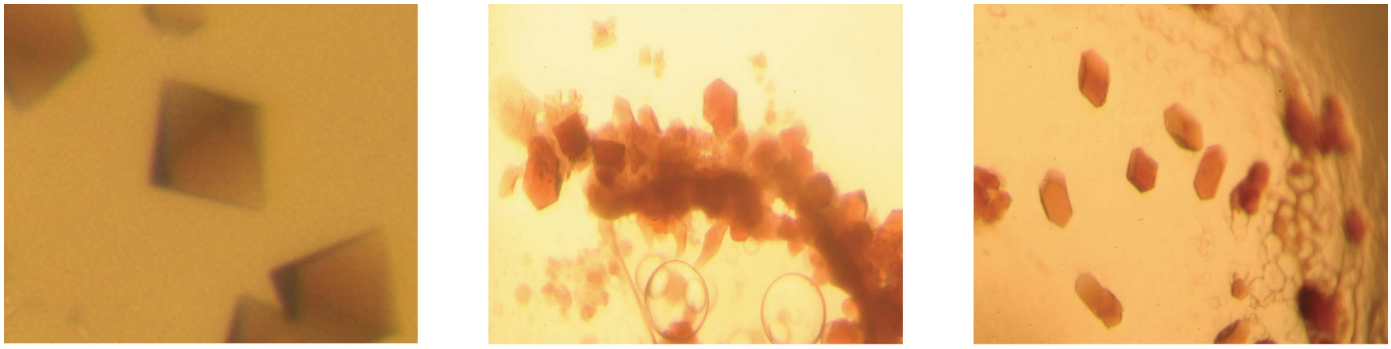

(*a*) (*b*) (*c*)

Figure 2
(*a*) Tetragonal bipyramidal crystals of recombinant *T. thermophilus* cytochrome ba_3 oxidase in space group $P4_32_12$; (*b*) rhombohedron-shaped crystals of the cytochrome ba_3 single mutant I-K258R in space group $P4_12_12$; (*c*) prismatic crystals of the cytochrome ba_3 double mutant I-K258R/II-E4Q in space group $P4_12_12$. The crystals are ∼0.2 mm along their longest axis.

2.4. Use of the *CCP*4 program *CONTACT*

Four structures, native *T. thermophilus* cytochrome ba_3 (PDB code 1ehk), recombinant cytochrome ba_3 (PDB code 1xme), single-mutant (PDB code 2qpd) and double-mutant (PDB code 2qpe) cytochrome ba_3 and *R. sphaeroides* cytochrome aa_3 (PDB code 2gsm), were analyzed to find symmetry-generated intermolecular contacts using the *CCP*4 program *CONTACT* (Collaborative Computational Project, Number 4, 1994). Potentially strong hydrogen-bonding interactions, *e.g.* those designated with three asterisks in the output, are shown in supplementary Tables S1–S4[1]. In these calculations the contact distance was set to <3.1 Å in order to emphasize the strongest interactions, although weaker interactions, which would be included within the program's normal default of <3.6 Å, also contribute to lattice stability.

3. Results and discussion

3.1. Introduction to the cytochrome ba_3 structure

Fig. 1 shows the overall structure of cytochrome ba_3. Note the arrangement of residues I-Lys258, I-Glu510 and II-Glu4, which reside in a small 'patch' on the relatively flat cytosol-facing surface of the enzyme and come into symmetric contact by a twofold rotation (see below).

3.2. General features of the mutants

Optical absorption spectra, electron-transfer activities (Keightley *et al.*, 1992) and low-temperature EPR spectra indicated that the proteins used in this study were complete and fully active as oxidases of *T. thermophilus* cytochrome c_{552}. The two mutant enzymes crystallize under the same conditions as the recombinant His-tagged wild-type protein, but differ in their crystallization properties. The wild-type protein formed square bipyramidal crystals belonging to space group $P4_32_12$ approximately one month after setup, whereas both mutant proteins crystallized after only 1–3 d as rhombohedra or irregular prisms belonging to space group $P4_12_12$ (Fig. 2).

The observed changes in packing evidently arise from the mutations. Unit-cell parameters and enzyme concentrations are presented in Table 2. Statements of diffraction resolution do not generally reveal how many crystals were mounted and analyzed before the reported value was obtained. In the case of the recombinant cytochrome ba_3, over 60 crystals were mounted before the reported 'hit' value was discovered (Hunsicker-Wang *et al.*, 2005). For the oxidized form of the double mutation it was necessary to screen ∼20 crystals to find a 'hit' of 2.6 Å; subsequently, all crystals diffracted to at least 3.5 Å resolution. We are exploring conditions that are expected to increase the number of well diffracting specimens and perhaps to provide even better resolution. Screens designed to detect different conditions for crystallization of these mutant proteins, as well as mutant forms prepared since the submission of this article, have revealed alternate crystallization conditions that will be described elsewhere.

3.3. New lattice packing

Fig. 3(*a*) shows the molecular packing of recombinant wild-type cytochrome ba_3 in space group $P4_32_12$ with its left-handed screw. This portion of the lattice contains 14 molecules of cytochrome ba_3 consisting of seven dimers, each superposed on the crystallographic twofold axis parallel to the (110) direction, *i.e.* the unit-cell diagonal in the plane of the *a* and *b* axes and normal to the *c* axis. Two of these axes emanate toward the viewer at intervals of *c*/2 (the vertical direction) in the view shown in Fig. 3(*a*). Repetition of the dimers by the left-handed fourfold screw axis parallel to *c* creates the contents of the unit cell. As noted above, monomers associate with each other by symmetric interaction of a 'patch' of three residues, I-Lys258, I-Glu510 and II-Glu4 (Fig. 4*a*), to form dimers. Although a similar overall packing arrangement occurs in crystals of native cytochrome ba_3 (Soulimane *et al.*, 2000), the shift in packing arising from the introduction of the His tag (Hunsicker-Wang *et al.*, 2005) increases the number of contacts from five to 14 (Tables S1 and S2[1]), including the new pair of salt bridges. Because this closely spaced pair of salt bridges extends throughout the lattice, we hypothesized that this interaction may be key to forming the crystal lattice.

Creating the I-K258R mutant of cytochrome ba_3 assumed that arginine might form a more stable salt bridge with I-Glu510, although the longer arginine side chain may also interfere with salt-bridge formation. The conversion of II-Glu4 to II-Gln4 was performed to reduce the net charge of the 'patch' to zero. Contrary to expectation, however, these mutations disrupted the twofold 'patch' interaction and forced a new arrangement of molecules manifested by the right-handed $P4_12_12$ space group (Table 2). The packing of ten molecules within this lattice is shown in Fig. 3(*b*).

A greater number of inter-protein contacts may facilitate the emergence of the new crystal form: 14 for recombinant wild-type cytochrome ba_3 (Table S2[1]), 34 for the single mutant (Table S3[1]) and 27 for the double mutant (Table S4[1]). These contacts contain

[1] Supplementary material has been deposited in the IUCr electronic archive (Reference: BW5212).

hydrophobic interactions; for example, the face-to-face hydrophobic contact of I-Pro499 with its symmetry partner on the twofold in the mutant forms (see Tables S3 and S4). Finally, the greater number of contacts per molecule may also result from the use of different symmetry operators (Tables S1, S2, S3 and S4), fortuitously providing greater stabilization of the lattice in all dimensions. Perhaps for these reasons, the new crystal form grows rapidly and reproducibly for both of the mutants.

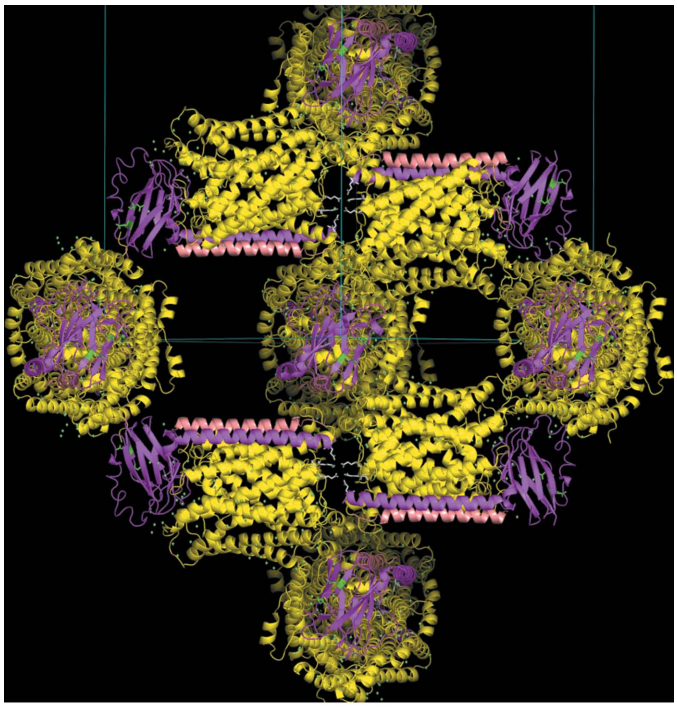

(*a*)

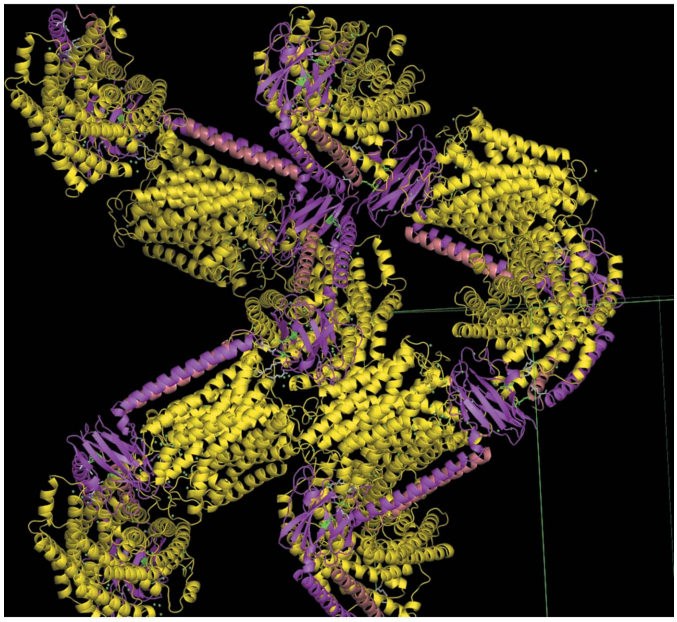

(*b*)

Figure 3
(*a*) Packing of 14 molecules of recombinant wild-type *T. thermophilus* cytochrome ba_3 (PDB code 1xme) in the left-handed space group $P4_32_12$; the five cylinders facing the reader are dimers, while two dimers lie horizontally in the plane. (*b*) Packing of ten molecules of either single-mutant or double-mutant cytochrome ba_3 in the right-handed space group $P4_12_12$; sets of five molecules exhibit 4_1 screw-axis symmetry. The color scheme is as given in the legend to Fig. 1. The cyan or green box in (*a*) or (*b*) represents the unit cell. In both (*a*) and (*b*) the view is along the (110) direction (unit-cell diagonal in the *ab* plane) and the *c* axis is vertical.

Table 2
Effect of the mutations on the crystallization of cytochrome ba_3 oxidase.

	Wild type	I-K258R	I-K258R/II-E4Q
PDB code	1xme	2qpd	2qpe
Space group	$P4_32_12$	$P4_12_12$	$P4_12_12$
Unit-cell parameters (Å)	$a = b = 114.90$, $c = 177.06$	$a = b = 115.19$, $c = 149.14$	$a = b = 114.64$, $c = 148.57$
Unit-cell volume (Å^3)	2.338×10^6	1.979×10^6	1.953×10^6
Matthews coefficient (Å^3 Da^{-1})	3.44	2.91	2.87
Solvent content (%)	64.24	57.76	57.19
Protein concentration† (m*M*)	5.7	6.7	6.8
Crystal morphology	Tetragonal bipyramidal	Rhomb-shaped	Prismatic

† Protein concentration in the unit cell as calculated from the unit-cell parameters and a molecular weight of ∼85 kDa.

In the single mutation, I-Arg258 interacts strongly (2.71 Å) with II-Glu4 of the same cytochrome ba_3 molecule and is 5.3 Å from the carbonyl group of II-Asn93 (see Fig. 4*b*). In comparison, in the double mutant I-Arg258 makes a new intermolecular interaction (2.97 Å) with the carbonyl of II-Asn93 and II-Glu4 makes a new intermolecular interaction (2.66 Å) with II-Glu96 OE2 (Fig. 4*c*). These new contacts (or near-contacts for the single mutant; Fig. 4*b*) involve polar residues on the soluble Cu_A domain, *i.e.* residues II-Asn93 and II-Glu96, and invoke the right-handed fourfold screw-axis symmetry operator (Tables S3 and S4). Furthermore, the contacts between the mutated 'patch' and the Cu_A domain occur simultaneously for each cytochrome ba_3 molecule, *i.e.* they are compatible with the 4_1 screw axis (all four: z, $z + 1/4$, $z + 1/2$, $z + 3/4$). Hence, each cytochrome ba_3 molecule spans one quarter of the *c*-axis dimension and is anchored by contacts at both ends as the molecules spiral head-to-tail around the 4_1 screw axis.

Both single-mutant and double-mutant proteins show an extensive set of new twofold contacts resulting from a different cytosol-facing loop of cytochrome ba_3: I-Arg496-Glu497-Arg498-Pro499-Lys500-Glu501 (not shown). This highly charged segment adopts an extended β-strand conformation and while there are no direct β-sheet-like hydrogen bonds across the twofold, the rings of I-Pro499 and its symmetry mate are packed face to face. The new twofold interaction also involves residues at the N-terminus of subunit I (I-Ser6, I-Glu7 and I-Arg10) and accommodates the disordered His tag into the solvent voids of the lattice as in the $P4_32_12$ crystal form (Hunsicker-Wang *et al.*, 2005).

3.4. Comparison of contact numbers

Analysis using *CONTACT* (Collaborative Computational Project, Number 4, 1994; Tables S1 and S2) shows that the molecules of native and recombinant wild-type cytochrome ba_3 have five and 14 inter-protein contacts (possible hydrogen bonds at <3.1 Å), respectively, between a given protein molecule and all others related by symmetry and/or lattice translations. As noted, the number of such contacts for the new crystal forms of the single and double mutants is 34 and 27, respectively (Tables S3 and S4). By the same criterion, the recent high-resolution structure of the enzyme from *R. sphaeroides* (Qin *et al.*, 2006) has only eight such potential contacts. It is noteworthy that the crystals of the latter protein grow in the presence of Cd^{2+} ions, which form bonds between molecules in the lattice and are likely to contribute to the 2.0 Å resolution diffraction (Qin *et al.*, 2006). Other crystals of cytochrome oxidases either have additional hydrophilic subunits (Tsukihara *et al.*, 1996; Qin *et al.*, 2006) or are incorporated

into a lattice as an antibody complex (Ostermeier *et al.*, 1995, 1997; Hunte & Michel, 2002). Hence, at present only the four cytochrome oxidase crystal structures analyzed here can be compared directly. As these crystal forms share the same number of symmetry operators, differing only in chirality ($P4_12_12$ *versus* $P4_32_12$), knowing the number of contacts per molecule in each lattice may be relevant to understanding the shift between them.

3.5. Rationalization of the unexpected results

In terms of the sole criterion of resolution, *i.e.* ignoring factors of yield, reproducibility and ease of cryoprotection, the number of contacts is not correlated with resolution: there are five contacts at 2.4 Å resolution (Soulimane *et al.*, 2000), 14 at 2.3 Å (Hunsicker-Wang *et al.*, 2005), 34 at 3.25 Å and 27 at 3.0 Å (Table 1). This may be a consequence of the overall paucity of specific interactions between the ∼80 kDa oxidases and within crystals of membrane proteins in general (Ostermeier & Michel, 1997; Soulimane *et al.*, 2003), possibly owing to occluding detergent micelles. However, the increased number of contacts in the engineered $P4_12_12$ crystal form does correlate with the rapidity and yield of crystal growth and robustness with respect to cryoprotection and consistent diffraction resolution. These observations raise the question as to why native and recombinant wild-type cytochrome ba_3 molecules do not rapidly achieve the lower free energy implied by the greater number of inter-protein contacts in the $P4_12_12$ space group. We speculate that the symmetry-related salt-bridged dimer of the wild-type proteins may form under the current conditions of crystallization, inhibiting the formation of the more stable $P4_12_12$ lattice and permitting the crystals to be constructed directly from the dimers observed in the $P4_12_12$ lattice. The propensity of dimers to crystallize has been demonstrated for the soluble protein T4 lysozyme (Banatao *et al.*, 2006). In contrast, the new twofold interaction in the $P4_12_12$ form, while extensive, lacks symmetric salt bridges. When the symmetric interaction 'patch' composed of I-Lys258, I-Glu510 and II-Glu4 is destabilized, as has clearly been caused by the mutations, the monomers may dominate and accrue into the more stable packing arrangement shown in Fig. 3(*b*). The latter scenario may also explain the shortened crystallization time.

As noted above, Pauth *et al.* (1999) modified suspected exterior residues in the *E. coli* outer membrane proteins OmpA171t (K107Y) and OmpXs (H100N). Each mutation permitted ready crystallization and allowed diffraction to <1.9 Å. In a subsequent communication, Pauth & Schulz (2000) reported the 1.65 Å structure of OmpA171t. Remarkably, Tyr107 makes neither intra-protein nor inter-protein contacts within the crystal lattice. Rather, this mutation places a neutral tyrosine side chain in nearest neighbor contact with the positively charged side chain of Lys113. A likely explanation of the Pauth *et al.* (1999) result with OmpA171t is that the K107Y mutation removes an electrostatic interaction between Lys107 and Lys113 that

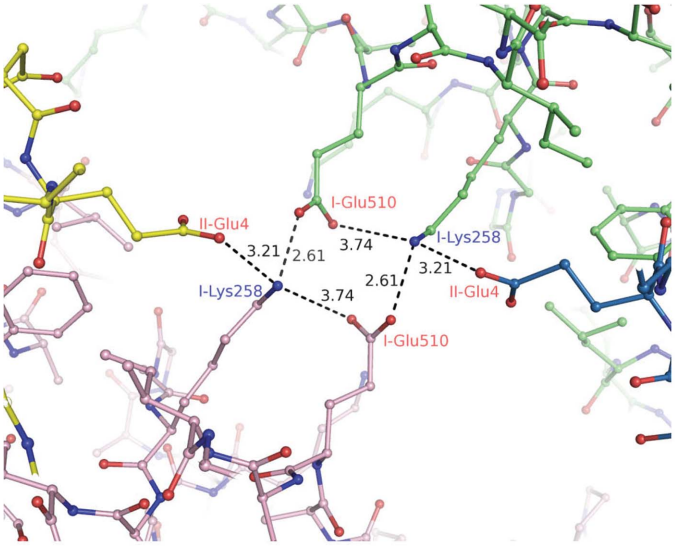

(*a*)

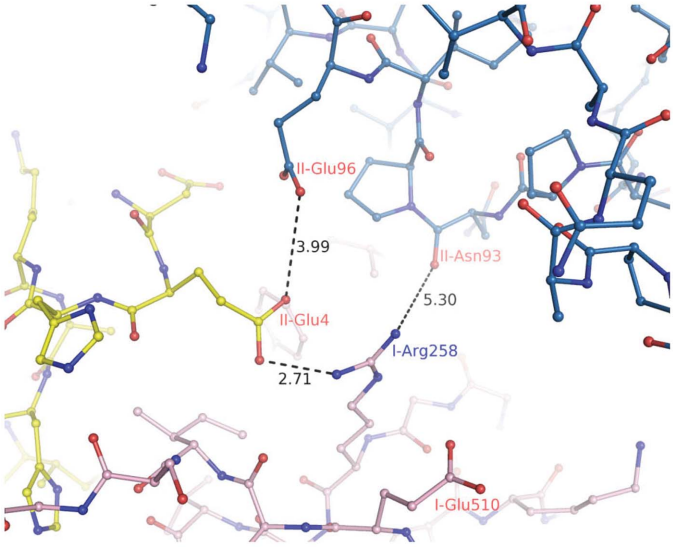

(*b*)

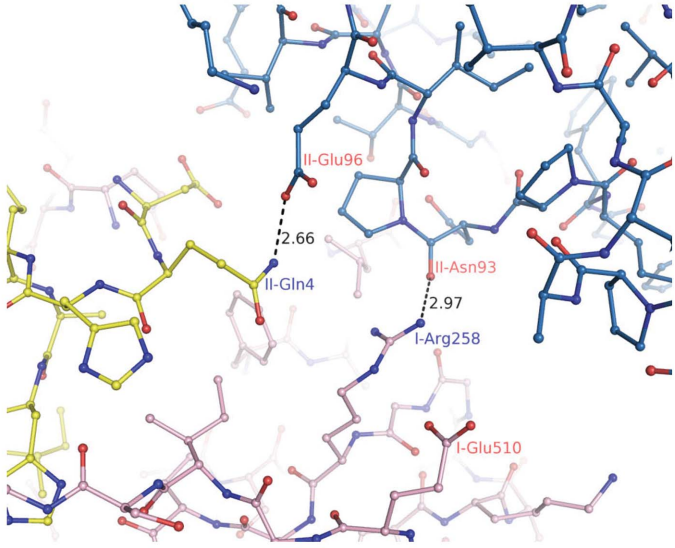

(*c*)

Figure 4
Lattice contacts in crystals of *T. thermophilus* cytochrome ba_3. In the recombinant wild-type structure (*a*), two salt bridges (2.61 Å in distance) between I-Lys258 NZ and I-Glu510 OE2 and between I-Glu510 OE2 and I-Lys258 NZ in the twofold symmetric mate were observed. In addition, hydrogen bonds are observed involving I-Lys258, I-Glu510 and II-Glu4 within each molecule. For the I-K258R mutant (*b*) a salt bridge (2.71 Å) between I-Arg258 NH1 and II-Glu4 OE2 is formed, while these residues are now proximal to subunit II of cytochrome ba_3. In the I-K258R/II-E4Q mutant structure (*c*) two new hydrogen bonds are observed: between II-Glu4 NE2 and II-Glu96 OE2 (2.66 Å) and between I-Arg258 NH2 and II-Asn93 O (2.97 Å). The latter interaction with the main chain of the Cu_A domain (subunit II) may contribute to the improved diffraction resolution of the double mutant (see Table 1). Subunits I and II in the reference molecule are shown in pink and yellow, respectively. For the symmetric mate, they are shown in green and blue, respectively.

is unfavorable to crystallization. Similar considerations of the OmpXs (H100N) structure (Vogt & Schulz, 1999) find that the carboxamide side chain of Asn100 in this protein may interact with its symmetry mate, resulting in a novel hydrogen-bonding arrangement (albeit twofold disordered) that could favorably affect crystallization properties. Indeed, such a possibility may be seen in the electron-density map available from the Protein Data Bank (PDB code 1qj8).

Our results, combined with those from the Schulz laboratory, suggest that polar surface modifications of integral membrane proteins, along the lines of those made with soluble proteins, may result in improved crystal properties. However, as borne out by these two cases, obtaining favorable results may depend heavily on good luck.

The work was supported by NIH grant GM 35342. We thank the support staff of SSRL for generous assistance. SSRL is operated by the Department of Energy, Office of Basic Energy Sciences. The SSRL Biotechnology Program is supported by the National Institutes of Health, National Center for Research Resources, Biomedical Technology Program and by the Department of Energy, Office of Biological and Environmental Research. Thanks also to Dr William Antholine of the NIH National Biomedical ESR Center for recording the EPR spectra.

References

Banatao, D. R., Cascio, D., Crowley, C. S., Fleissner, M. R., Tienson, H. L. & Yeates, T. O. (2006). *Proc. Natl Acad. Sci. USA*, **103**, 16230–16235.
Chen, Y., Hunsicker-Wang, L., Pacoma, R. L., Luna, E. & Fee, J. A. (2005). *Protein Expr. Purif.* **40**, 299–318.
Collaborative Computational Project, Number 4 (1994). *Acta Cryst.* D**50**, 760–763.
Cooper, D. R., Boczek, T., Grelewska, K., Pinkowska, M., Sikorska, M., Zawadzki, M. & Derewenda, Z. (2007). *Acta Cryst.* D**63**, 636–645.
Czepas, J., Devedjiev, Y., Krowarsch, D., Derewenda, U., Otlewski, J. & Derewenda, Z. S. (2004). *Acta Cryst.* D**60**, 275–280.
D'Arcy, A., Stihle, M., Kostrewa, D. & Dale, G. (1999). *Acta Cryst.* D**55**, 1623–1625.
Dasgupta, S., Iyer, G. H., Bryant, S. H., Lawrence, C. E. & Bell, J. A. (1997). *Proteins*, **28**, 494–514.
DeLano, W. L. (2002). *The PyMOL Molecular Graphics System.* http://www.pymol.org.
Derewenda, Z. S. (2004*a*). *Methods*, **34**, 354–363.
Derewenda, Z. S. (2004*b*). *Structure*, **12**, 529–535.
Derewenda, Z. S. & Vekilov, P. G. (2006). *Acta Cryst.* D**62**, 116–124.
Elberry, M., Xiao, K., Esser, L., Xia, D., Yu, L. & Yu, C. A. (2006). *Biochim. Biophys. Acta*, **1757**, 835–840.
Hunsicker-Wang, L. M., Pacoma, R. L., Chen, Y., Fee, J. A. & Stout, C. D. (2005). *Acta Cryst.* D**61**, 340–343.
Hunte, C. & Michel, H. (2002). *Curr. Opin. Struct. Biol.* **12**, 503–508.
Keightley, J. A., Mather, M. W., Springer, P. & Fee, J. A. (1992). *FASEB J.* **6**, Abstract No. 1114.
Lawson, D. M., Artymiuk, P. J., Yewdall, S. J., Smith, J. M., Livingstone, J. C., Treffry, A., Luzzago, A., Levi, S., Arosio, P. & Cesareni, G. (1991). *Nature (London)*, **349**, 541–544.
Leslie, A. G. W. (1999). *Acta Cryst.* D**55**, 1696–1702.
Longenecker, K. L., Garrard, S. M., Sheffield, P. J. & Derewenda, Z. S. (2001). *Acta Cryst.* D**57**, 679–688.
Mateja, A., Devedjiev, Y., Krowarsch, D., Longenecker, K., Dauter, Z., Otlewski, J. & Derewenda, Z. S. (2002). *Acta Cryst.* D**58**, 1983–1991.
Michel, H., Behr, J., Harrenga, A. & Kannt, A. (1998). *Annu. Rev. Biophys. Biomol. Struct.* **27**, 329–356.
Mittl, P. R. E., Berry, A., Scrutton, N. S., Perham, R. N. & Schulz, G. E. (1994). *Acta Cryst.* D**50**, 228–231.
Murshudov, G. N., Vagin, A. A. & Dodson, E. J. (1997). *Acta Cryst.* D**53**, 240–255.
Ostermeier, C., Harrenga, A., Ermler, U. & Michel, H. (1997). *Proc. Natl Acad. Sci. USA*, **94**, 10547–10553.
Ostermeier, C., Iwata, S., Ludwig, B. & Michel, H. (1995). *Nature Struct. Biol.* **2**, 842–846.
Ostermeier, C. & Michel, H. (1997). *Curr. Opin. Struct. Biol.* **7**, 697–701.
Pauth, A. & Schulz, G. E. (2000). *J. Mol. Biol.* **298**, 273–282.
Pauth, A., Vogt, J., Model, K., Siebold, C. & Schulz, G. E. (1999). *Proteins*, **34**, 167–172.
Qin, L., Hiser, C., Mulichak, A., Garavito, R. M. & Ferguson-Miller, S. (2006). *Proc. Natl Acad. Sci. USA*, **103**, 16117–16122.
Read, R. J. (2001). *Acta Cryst.* D**57**, 1373–1382.
Schlatter, D., Thoma, R., Küng, E., Stihle, M., Müller, F., Borroni, E., Cesura, A. & Hennig, M. (2005). *Acta Cryst.* D**61**, 513–519.
Soulimane, T., Buse, G., Bourenkov, G. P., Bartunik, H. D., Huber, R. & Than, M. E. (2000). *EMBO J.* **19**, 1766–1776.
Soulimane, T., Kiefersauer, R. & Than, M. E. (2003). *Membrane Protein Purification and Crystallization: A Practical Guide*, edited by C. Hunte, G. von Jagow & H. Schägger, pp. 229–251. Amsterdam: Academic Press.
Takeda, S., Yoshimura, H., Endo, S., Takahashi, T. & Nagayama, K. (1995). *Proteins*, **23**, 548–556.
Tsukihara, T., Aoyama, H., Yamashita, E., Tomizaki, T., Yamaguchi, H., Shinzawa-Itoh, K., Nakashima, R., Yaono, R. & Yoshikawa, S. (1996). *Science*, **272**, 1136–1144.
Vogt, J. & Schulz, G. E. (1999). *Structure*, **7**, 1301–1309.